

TIME-DEPENDENT SIMULATIONS OF SHEAR-THINNING ELASTIC FLOWS THROUGH CONTRACTIONS

Paulo J. Oliveira

Departamento de Engenharia Electromecânica
Universidade da Beira Interior, 6201-001 Covilhã, Portugal
pipo@ubi.pt

ABSTRACT

Past numerical work with constant-viscosity viscoelastic fluids through planar contractions has enabled steady-state solutions to be obtained at relatively high Weissenberg numbers (We up to 10). Those solutions for the upper-convected Maxwell and Oldroyd-B models showed steady flow patterns for increasing We with the appearance of lip-vortices, vortex growth, and corner-lip vortex merging, in agreement with recent simulations and some experimental work. When similar simulations were performed with two shear-thinning viscoelastic models, namely the Phan-Thien – Tanner and the Giesekus models, steady state solutions could not be obtained beyond a certain value of We , but the solution was seen to follow a periodic unsteady flow pattern. The present paper reports preliminary numerical results which highlight the formation of the lip vortices through a sequence of time dependent events.

INTRODUCTION

When viscoelastic liquids flow through ducts or tubes with sudden reduction in cross section, large corner vortices appear at the entrance to the smaller duct or tube. Both the dimensions of these vortices and the intensity of the entrapped recirculating flow are much larger than that occurring with Newtonian liquids in equivalent conditions, and tend to increase with elasticity and decrease with inertia. An early review of the problem of viscoelastic fluid flow through contractions can be found in Boger (1987). The phenomenon is further complicated by appearance of a different type of

vortices known as “lip vortices” which are located around the reentrant corner, at the edge of the opening to the smaller duct, and only exist under certain flow conditions (We and Re) and tend to grow and join the corner vortices; they have been observed experimentally (Boger et al., 1986 and Evans and Walters, 1986) and captured by numerical simulations (Xue et al., 1998; Oliveira and Pinho, 1999b).

Most of the numerical simulations have been with fluid models having a constant shear viscosity, like the upper-convected Maxwell (UCM) and Oldroyd-B models, and steady solutions were obtained up to relatively high Weissenberg numbers (Oliveira et al., 1999a,b; Alves et al., 2000). We have also done a few computations with the Phan-Thien and Tanner's (1977) PTT model, which has a shear thinning viscosity, but only in a restricted range of We ($We=2$). Others have used the PTT model in wider range of We (Carew et al., 1993) but their methods were applied with computational meshes which were rather coarse.

In this paper, we present preliminary numerical results regarding the behaviour of the PTT and Giesekus (1982) fluids through planar contractions with an area ratio of 4-to-1, which provide evidence that the process of formation and growth of lip vortices is inherently time-dependent. Our time-marching solution algorithm was able to naturally capture that time-dependent pulsating phenomena, which repeats itself over and over with a given well-defined period. Results for the PTT model have been presented in a recent conference of the Portuguese Society of Rheology (Oliveira, 2001) and here we add related findings for a different, but commonly used, constitutive model (the Giesekus' model). It should be noted that time instabilities in lip vortex formation have been observed in many experiments, see e.g. Boger et al. (1986) and

McKinley et al. (1991); for example, Boger and Walters (1993) in their book show very nice photographs (originated from Binnington) of a pulsating lip vortex with similarities to our time-dependent results.

EQUATIONS AND METHOD

The incompressible flow of viscoelastic liquids is governed by the usual conservation equations for mass:

$$\nabla \cdot \mathbf{u} = 0 \quad (1)$$

and momentum:

$$\frac{\partial \rho \mathbf{u}}{\partial t} + \nabla \cdot \rho \mathbf{u} \mathbf{u} = -\nabla p + \nabla \cdot \boldsymbol{\tau} \quad (2)$$

where \mathbf{u} is the velocity, ρ the density and p the pressure. A rheological equation of state is required to specify the extra stress tensor $\boldsymbol{\tau}$ in terms of the kinematics of the flow. In this study two well-known models are considered, the simplified form of the PTT model used by Xue et al (1998):

$$(1 + \frac{\lambda \epsilon}{\eta} \text{tr} \boldsymbol{\tau}) \boldsymbol{\tau} + \lambda \overset{\nabla}{\boldsymbol{\tau}} = 2 \eta \mathbf{D} \quad (3)$$

and the Giesekus (1982) model:

$$\boldsymbol{\tau} + \lambda \overset{\nabla}{\boldsymbol{\tau}} + \frac{\alpha \lambda}{\eta} \boldsymbol{\tau} \cdot \boldsymbol{\tau} = 2 \eta \mathbf{D} \quad (4)$$

As it is apparent, both are non-linear in $\boldsymbol{\tau}$ due to the terms multiplied by the model parameters ϵ and α and a consequence is that both exhibit shear thinning of viscosity. In the above equations, Oldroyd's upper convected derivative is given by:

$$\overset{\nabla}{\boldsymbol{\tau}} \equiv \frac{\partial \boldsymbol{\tau}}{\partial t} + \nabla \cdot \mathbf{u} \boldsymbol{\tau} - \nabla \mathbf{u}^T \cdot \boldsymbol{\tau} - \boldsymbol{\tau} \cdot \nabla \mathbf{u}$$

and the rate of strain tensor is denoted:

$$\mathbf{D} \equiv \frac{1}{2}(\nabla \mathbf{u} + \nabla \mathbf{u}^T).$$

Besides ϵ and α , those models are characterised by two other constant parameters, the relaxation time λ and the viscoelastic viscosity η . Under the simplified forms here considered, no retardation time is included and so there is no purely viscous contribution to the total stress. Therefore, when either ϵ or α tend to zero, the models reduce to the UCM equations and not to the Oldroyd-B.

A collocated finite-volume method (FVM) is employed to solve the above set of coupled differential equations. Equations (1)-(4) are integrated over control-volumes (V) forming the

computational mesh, are linearised, and are transformed into algebraic equations of the form:

$$\sum_f^6 F_f = 0 \quad (5)$$

$$a_P \mathbf{u}_P = \sum_F^6 a_F \mathbf{u}_F + S_u \quad (a_P = \frac{\rho V}{\delta t} + a_0) \quad (6)$$

$$a_P^T \boldsymbol{\tau}_P = \sum_F^6 a_F^T \boldsymbol{\tau}_F + S_\tau \quad (7)$$

Here, F_f are mass flow rates across cell face f (in-between cells P and F), a_F and a_F^T are coefficients in the momentum and stress equations accounting for convection and diffusion influences, $a_0 = \sum_F a_F$, and S are source terms. A diffusion term is added and subtracted to the right-hand side of Eq. (2). The central coefficient of the stress equation, a_P^T , is given by different expressions for the two constitutive equations. For the SPTT it is:

$$a_P^T = \frac{\lambda V}{\delta t} + a_0^T + V(1 + \frac{\lambda \epsilon}{\eta} \text{tr} \boldsymbol{\tau}_P) \quad (8)$$

where the first term arises from the time-dependent term in the original equation, the second term is $a_0^T = \sum_F a_F^T$ with the coefficients composed only by convection fluxes, and the last two terms are very helpful in that serve to enhance diagonal dominance of the final matrix equations. Of course, this is only possible because the trace of $\boldsymbol{\tau}$ is always positive.

For the Giesekus model it is not so clear how to retain the wanted diagonal-dominance, but that can be achieved as explained in Oliveira (2001), resulting in the following expression for the central coefficient:

$$a_P^T = \frac{\lambda V}{\delta t} + a_0^T + V(1 + \frac{\lambda \alpha}{\eta} \text{tr} \boldsymbol{\tau}_P). \quad (9)$$

Other details of this FVM can be found in Oliveira and Pinho (1999a). The method is fully implicit in time, since the time derivative was represented by the first-order backward Euler scheme. Spatial interpolation schemes are basically second-order, based on central differencing, except the convection terms which can be based on various higher-order schemes (see Alves et al., 2000) but here the basic first-order upwind scheme is adopted. Upwind is known to introduce numerical diffusion into the solution and this can be especially troublesome for the hyperbolic stress Eq. (7). However, that effect is not detrimental to the validity of the present results as increased diffusion would act to mask any time-dependency.

It is emphasised that the time-dependent terms in Eqs. (6) and (7) are usually retained to act as inertial-relaxation when

steady solutions are sought but, if the time step (δt) is small enough, the actual time dependent behaviour of a developing flow can be captured. Due to the nonlinearities and inter linkage between velocity and pressure, and kinematics and stress, the overall scheme here employed can only be first-order, at best. Improved accuracy requires iteration within a time step, and a better representation of the time derivative. This work is now under way.

FLOW CONFIGURATION AND MESHES

The flow geometry is represented in Fig. 1. H is the half-width of the downstream duct, where the average velocity is U . A Weissenberg number is defined as $We = \lambda U/H$ and a Reynolds number as $Re = \rho UH/\eta$. In order to minimise inertia effects, the Reynolds number was kept at a low value of $Re = 0.01$, while the We was raised up to a level at which a steady solution could not be obtained and the norm of the residuals of the equations were found to follow a time-periodic evolution. A constant value typical of polymer melts (e.g. Carew et al., 1993) was assigned to the elongational parameter of the PTT model, $\epsilon = 0.25$, while for the Giesekus model we take the widely used value of $\alpha = 0.5$ (for which the model is sometimes referred to as the Leonov model).

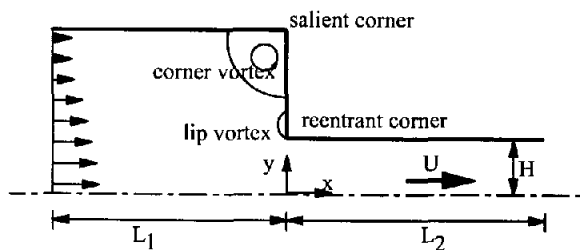


Figure 1. Sketch of the flow domain.

In terms of mesh resolution, computations for the PTT model have been carried out in the fine mesh of Oliveira and Pinho (1999a), with upstream and downstream duct lengths of $L_1 = L_2 = 10H$, and for the Giesekus model we used the medium mesh of that reference. The Giesekus model is more shear thinning than the PTT, has a non-zero second normal stress coefficient, and these two features lead to more difficult numerical treatment. In future work we expect to test that same model in finer meshes but the purpose here is not so much related to accuracy. In the finer mesh the total number of CVs is 11760 and the minimum mesh spacing near the reentrant corner is $\delta x_{\min} = \delta y_{\min} = 0.01 H$, while the medium mesh has the double of this minimum mesh spacing

(0.02). Such non-uniform meshes with higher concentration of CVs around the corner are necessary to resolve the steep stress gradients provoked by that geometrical singularity and are also beneficial to eventually resolve the lip vortices.

Table 1. Vortex characteristics for the PTT and UCM fluids

We	ϵ	Ψ_{\max}	X_R	$\tau_{zz,\max}$	ϵ	Ψ_{\max}	X_R	$\tau_{zz,\max}$
0	—	1.00117	1.495	1.08	—	—	—	—
1	0.25	1.00141	1.545	10.2	0.0	1.00083	1.375	52.
2	"	1.00229	1.701	8.3	"	1.00077	1.308	98.
3	"	1.00372	1.882	7.39	"	1.00193	1.363	145.
4	"	1.00530	2.045	6.63	"	1.00371	1.505	195.
6	"				"	1.01026	1.891	296.
8	"				"	1.01632	2.263	445.

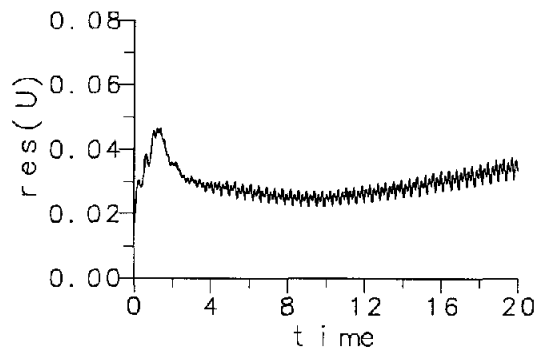


Figure 2. Decay of the u -residuals, starting from solution at $We=4$; time scaled with H/U . PTT fluid.

RESULTS FOR PTT MODEL

The vortex pattern upstream of the contraction plane can be characterised by two integral quantities: the maximum stream function Ψ_{\max} (a measure of the recirculation intensity) and the distance from the detachment point to the salient corner (a measure of the corner vortex size). Table 1 gives these values for We ranging from 0 (Newtonian flow) to 4, together with maximum values of the axial normal stress (scaled with $\eta U/H$). For comparison purposes, the corresponding values for the UCM fluid ($\epsilon = 0$) are given on the right-hand side of the Table; while the PTT values are limited to $We \leq 4$, since for the case $We=5$ the flow was found to be periodic, as discussed next, for the UCM steady results were found up to $We=8$. The strong shear-thinning characteristic of the PTT is reflected in the results of Table 1, with much lower levels of normal stresses, as compared with the UCM, and larger and more intense corner vortices without the presence of lip vortices for We up to 4. Lip vortices are present for the UCM case in the range $We=1-3$ (see Oliveira and Pinho 1999b) and absent for the PTT.

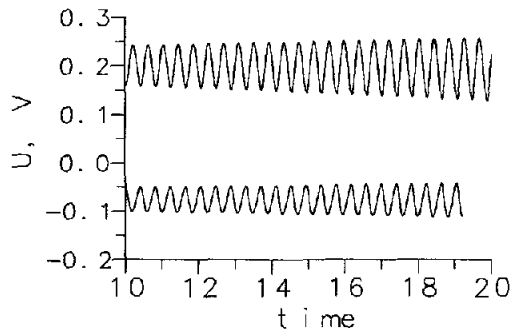


Figure 3. Time evolution of the u and v velocity component at the cell near the reentrant corner (velocity scaled with U , time with H/U). PTT fluid.

Based on our previous simulations we were expecting to obtain steady-state results for the PTT model at $We=5$ and higher, as shear thinning reduces the stresses and improves the numerical behaviour of the method. However, when the PTT case for $We=5$ was started from the solution for $We=4$, with the same time step ($\delta t = 0.25 \times 10^{-2} H/U$), it was found that a steady solution could not be achieved, even if the time step was lowered. Instead, the residuals of the equations did exhibit a periodic variation, as shown in Fig. 2. At that stage the solution itself was time-dependent and periodic, as exemplified by the variation of the longitudinal and lateral velocity components at a point very close to the reentrant corner, shown in Fig. 3. It is noteworthy that this periodic motion was established naturally, after an initial transient delay which took several characteristic times H/U (≈ 5), and presents a period of about $0.33 H/U$ (some 130 time steps). In terms of a Strouhal number defined as $Sr = \text{freq.} \times U/H$, we have $Sr \approx 3.0$.

The flow pattern near the contraction entrance during a full period of the pulsating regime is depicted in Figs. 4 (a)-(h), where each figure is separated by a time gap of 20 time steps. Streamlines inside and outside the recirculation are equally spaced and thus give a faithful indication of the relative vortex strength, which is given by the number above each figure ($\times 10^{-3}$). In Fig. 4 (a) a newly formed lip vortex is already enveloped by the separating streamline ($\Psi = 1$) and is engulfed into the corner vortex (b and c), which seems to become completely separated from the channel walls (d) (in a pulsating fashion). In Fig. 4 (e) another lip vortex is about to be formed on the smaller channel wall just downstream of the reentrant corner, it grows (f), and is pulled back (g-h) (by elasticity ?) into the larger channel where it joins the corner vortex. From that point, the sequence described before is

repeated, and this overall pulsating process repeats itself over and over for each period. We note that this time dependent behaviour would tend to be masked by numerical diffusion introduced by the discretization schemes. The fact that it is captured, in spite of the schemes utilised, gives some support to the belief that it represents real flow behaviour.

RESULTS FOR GIESEKUS MODEL

The above results led us to try a different constitutive model in order to check if the time dependent behaviour was only specific to the PTT, or eventually to some undesirable numerical effect. For these reasons we decided to simulate the flow of a Giesekus fluid with $\alpha = 0.5$ through the same contraction. For $We = 1$, we could obtain a steady solution with the residuals of the equations decaying to vanishing levels, and the velocity and stresses at a monitoring point tending to constant, steady values. However, for $We = 2$ a pulsating flow pattern would naturally establish itself, being especially noticeable in the region around the reentrant corner. So the situation is similar to that with the PTT model.

A plot of the variation with time of the u -momentum residuals is shown in Fig. 5. The time origin is arbitrary, as this run was restarted from the corresponding solution for the UCM fluid (at $We=2$), and the oscillatory pattern seen in Fig. 5 was established after a certain initial transient (of about 5000 time steps). The time step used in these calculations was 0.005. Figure 6 shows the variation of the u and v velocity components at the monitoring point (near the reentrant corner). Large repetition periods are observed for both velocity components. Due to strong shear-thinning, the flow is locally accelerated towards the re-entrant corner wall, at the entrance to the small channel. This gives rise to the high velocities in that region ($u > U$).

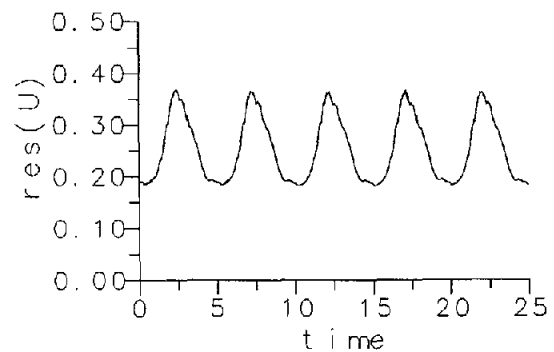


Figure 5. Variation with time of the u -residuals, for the Giesekus fluid at $We = 2$.

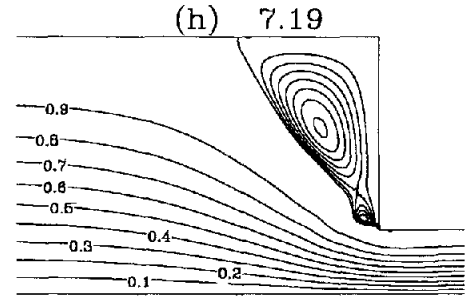
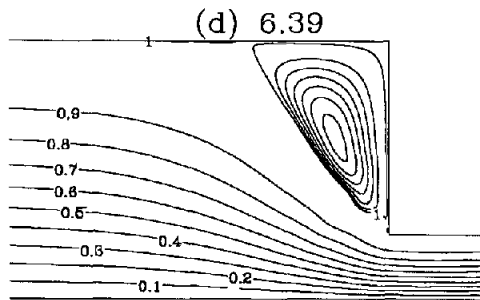
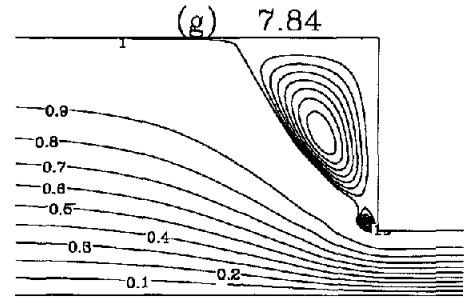
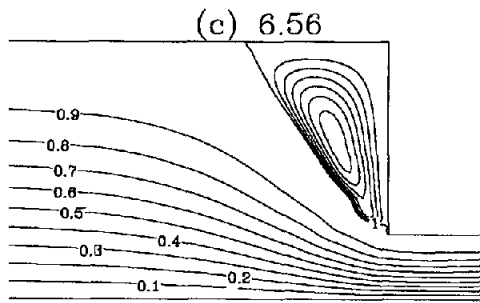
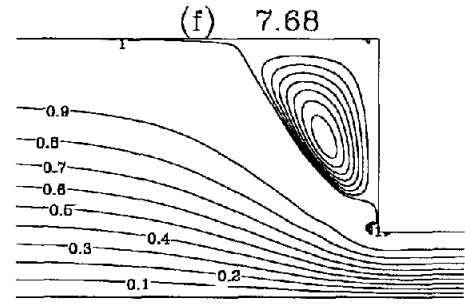
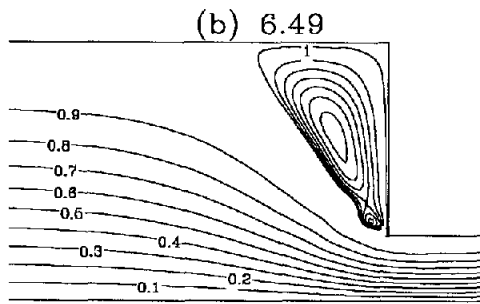
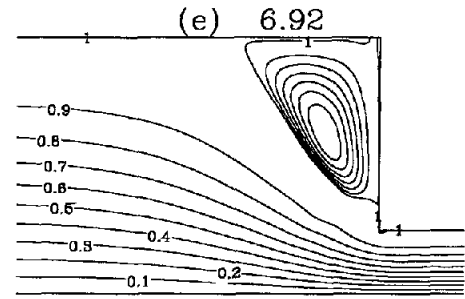
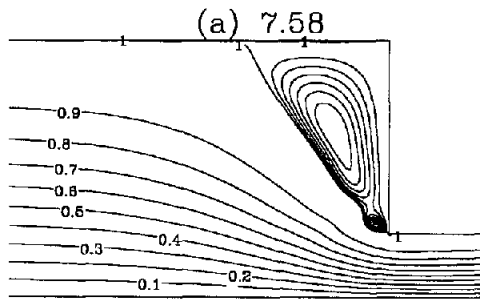


Figure 4. Streamline patterns for the PTT fluid at equally spaced moments in time, following the periodic motion (stream function scaled with inlet flow rate; interval

between frames 20 time steps; value above figures equal to $(\Psi_{\max} - 1) \times 10^3$).

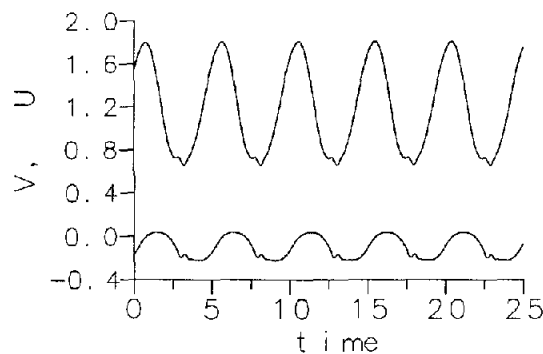


Figure 6. Variation with time of the u and v velocity components near the corner, for the Giesekus fluid at $We = 2$.

A “motion” picture of the flow field in the contraction is shown in Fig. 7, where the various streamline patterns (from (a) to (j)) are separated by a time gap of 0.5 (100 time steps). Due to the less refined mesh the streamlines are not as smooth as before, but the appearance and coalescence process of the lip vortex formation is similar to that found for the PTT fluid. As alluded above, shear-thinning is stronger for the Giesekus fluid, compared with the PTT, and consequently the flow distortion at the entrance to the narrow channel is higher in Fig. 7 than in Fig. 4. The period is now much longer than for the PTT, being approximate 5 in dimensionless time units (cf. Figs. 5 and 6), and so the 10 plots of Fig. 7 cover one period.

REFERENCES

- Alves, M.A., Pinho, F.T., and Oliveira, P.J., 2000, “Effect of a High-Resolution Differencing Scheme on Finite-Volume Predictions of Viscoelastic Flows”, *J. Non-Newtonian Fluid Mech.*, Vol. 93, pp. 287-314.
- Boger, D.V., 1987, “Viscoelastic Flows Through Contractions”, *Annual Rev. Fluid Mech.*, Vol. 19, pp. 157-182.
- Boger, D.V., Hur, D.U., and Binnington, R.J., 1986, “Further Observations of Elastic Effects in Tubular Entry Flows”, *J. Non-Newtonian Fluid Mech.*, Vol. 20, pp. 31-49.
- Boger, D.V., and Walters, K., 1993, “Rheological Phenomena in Focus”, *Rheology Series*, Vol. 4, Elsevier.
- Carew, E.O.A., Townsend, P., and Webster, M.F., 1993, “A Taylor-Petrov-Galerkin Algorithm for Viscoelastic Flow”, *J. Non-Newtonian Fluid Mech.*, Vol. 50, pp. 253-287.
- Evans, R.E., and Walters, K., 1986, “Further remarks on the lip-vortex mechanism of vortex enhancement in planar-contraction flows”, *J. Non-Newtonian Fluid Mech.*, 32, 95.
- Giesekus, H., 1982, “A Simple Constitutive Equation for Polymer Fluids Based on the Concept of the Deformation Dependent Tensorial Mobility”, *J. Non-Newtonian Fluid Mech.*, Vol. 11, pp. 69-109.
- McKinley, G.H., Raiford, W.P., Brown, R.A., and Armstrong, R.C., 1991, “Nonlinear Dynamics of Viscoelastic Flow in Axisymmetric Abrupt Contractions”, *J. Fluid Mech.*, Vol. 223, pp. 411-456.
- Oliveira, P.J., and Pinho, F.T., 1999a, “Numerical Procedure for the Computation of Fluid Flow with Arbitrary Stress-Strain Relationships”, *Numerical Heat Transfer, Part B: Fundamentals*, Vol. 35, pp. 295-315.
- Oliveira, P.J., and Pinho, F.T., 1999b, “Plane Contraction Flows of Upper Convected Maxwell and Phan-Thien – Tanner Fluids as Predicted by a Finite-Volume Method”, *J. Non-Newtonian Fluid Mech.*, Vol. 88, pp. 63-88.
- Oliveira, P.J., 2001, “Interesting Observations in the Numerical Simulation of Shear-Thinning Elastic Flows Through Contractions”, *Proc. 3rd Meeting Port. Soc. of Rheo.*, Instituto Piaget, pp. 97-102.
- Oliveira, P.J., 2001, “On the Numerical Implementation of Non-Linear Viscoelastic Models in a Finite-Volume Method”, *Numer. Heat Transf B: Fundamentals*, in press.
- Phan-Thien, N., and Tanner, R.I., 1977, “A New Constitutive Equation Derived from Network Theory”, *J. Non-Newtonian Fluid Mech.*, Vol. 2, pp. 353-365.
- Xue, S.-C., Phan-Thien, N., and Tanner, R.I., 1998, “Three Dimensional Numerical Simulations of Viscoelastic Flows Through Planar Contractions”, *J. Non-Newtonian Fluid Mech.*, Vol. 74, pp. 195-245.

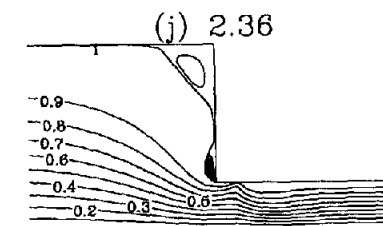
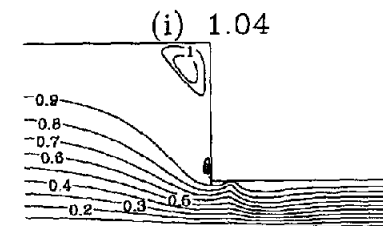
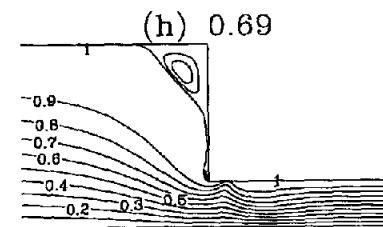
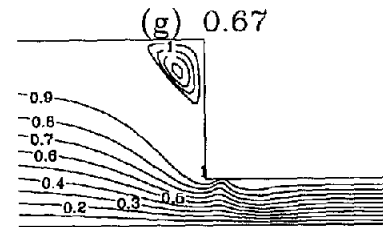
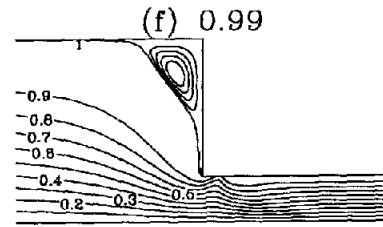
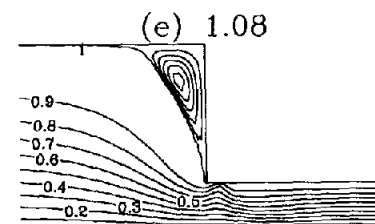
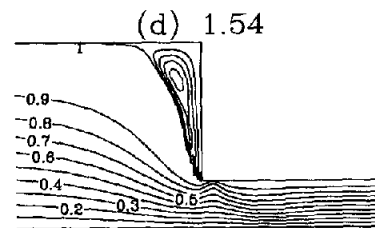
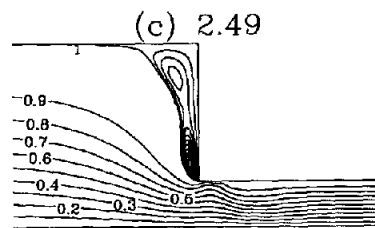
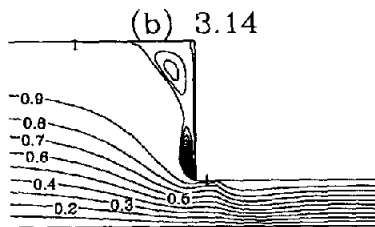
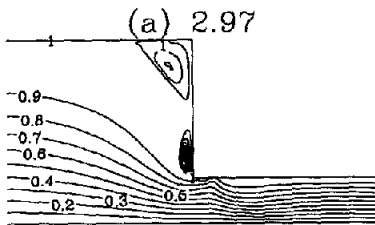


Figure 7. Time history of the flow pattern for the Giesekus fluid at $We = 2$.

From (a) to (j), graphs are separated by a time gap of 0.5; values over figures are $(\Psi_{\max} - 1) \times 10^3$.